Rigid body dynamic response of a floating offshore wind turbine to waves
Identification of the instantaneous centre of rotation through analytical and numerical analyses

Patryniak, Katarzyna; Collu, Maurizio; Coraddu, Andrea

Rigid body dynamic response of a floating offshore wind turbine to waves: Identification of the instantaneous centre of rotation through analytical and numerical analyses

Katarzyna Patryniak [a],*, Maurizio Collu [a], Andrea Coraddu [b]

[a] Department of Naval Architecture, Ocean and Marine Engineering, University of Strathclyde, Montrose St, Glasgow, G4 0LZ, UK
[b] Faculty of Mechanical, Maritime and Materials Engineering, Delft University of Technology, Mekelweg, Delft, 2628 CD, Netherlands

ARTICLE INFO

ABSTRACT

Floating Offshore Wind Turbines (FOWT) can harness the abundant offshore wind resource at reduced installation requirements. However, a further decrease in the development risks through higher confidence in the design and analysis methods is needed. The dynamic behaviour of FOWT systems is complex due to the strong interactions between the large translational and rotational motions and the diverse loads, which poses a challenge. While the methods to study the FOWT's general responses are well established, there are no methods to describe the highly complex time-dependent rotational motion patterns of FOWT. For a rigid body in general plane motion, an Instantaneous Centre of Rotation (ICR) can be identified as a point at which, at a given moment, the velocity is zero. However, it is common to assume a centre of rotation fixed in space and time, arbitrarily set at the centre of floatation or gravity. Identification of the ICR is crucial as it may lead to better motion reduction methods and can be leveraged to improve the designs. This includes better-informed fairlead placement and the reduction of aerodynamic load variability. In this paper, we propose a two-fold approach for the identification of the ICR: an analytical solution in the initial static equilibrium position, and a time-domain numerical approach for dynamic analysis in regular and irregular waves to understand the motion patterns and ICR sensitivity to environmental conditions. Results show that the ICR of FOWT depends on wave frequency and, at low frequencies, on wave height, due to the nonlinear viscous drag and mooring loads. An unexpected but interesting result is that the surge-heave-pitch coupling introduced by the mooring system leads to a dynamic phenomenon of signal distortion known as "clipping" in the nonlinear audio signal processing area, which, through the introduction of higher harmonics, is responsible for the ICR sensitivity to motion amplitude.

1. Introduction

1.1. Context

The global energy system is undergoing accelerated transformation to reach the internationally agreed climate objectives [1]. Renewable power technologies are leading this transformation, dominating the new generation capacity, mainly driven by the increase in wind and solar power generation [1]. Despite the astonishingly rapid growth in both onshore and offshore installations, wind energy is still off track to achieve the 2050 targets [2]. In recent years, the potential of the Floating Offshore Wind Turbines (FOWT) has been recognised: reduced installation requirements and capability to harness the abundant offshore wind resource led to a plethora of new, large-scale wind farm projects. However, further reduction of the life-cycle cost is essential

for the success of this technology [3]. This, in turn, requires the reduction of the development risks, which, among other factors, can be achieved through increased confidence in the design and analysis methods.

The dynamic response of highly-coupled FOWT systems to external loads is complex and so its numerical modelling is challenging, which can be seen in a wealth of recent literature. Particular attention has been given to studying the first and second-order hydrodynamic loads in varying environmental conditions [4,5], complex aerodynamics during platform motion [6–8], fluid–structure interaction (or hydroelasto-plasticity) [9,10], and control methods [11,12]. As the understanding of the general principles of FOWT dynamics improves, more and more in-depth analysis is being performed to examine the exact mechanisms driving FOWT responses in a complex environment.

Abbreviations and Nomenclature

$\mathbf{A}$	Hydrodynamic added mass matrix
A_i	ith cross-section area
A_{WP}	Waterplane area
$\mathbf{C}$	Stiffness matrix
C_A	Added mass coefficient
DOF	Degree(s) of Freedom
$E(x)$	Expected Value of x
$\boldsymbol{\eta}$	Platform displacement vector
FFT	Fast Fourier Transform
FOWT	Floating Offshore Wind Turbine(s)
FPSO	Floating Production Storage and Offloading
ICR	Instantaneous Centre of Rotation
I_{WL}	Second moment of waterplane area
I_{yy}	Second mass moment of inertia in pitch direction
m	Mass of the system
$\mathbf{M}$	Mass matrix
m_A	Sectional (2D) added mass
NREL	National Renewable Energy Laboratory
ω	Wave frequency
$\boldsymbol{\omega}$	Eigenvalues vector
O&G	Oil and Gas
RAO	Response Amplitude Operator
ρ	Water density
RNA	Rotor-Nacelle Assembly
R_i	ith cross-section radius
$\mathbf{r_{P_1,P_2}}$	Displacement between P_1 and P_2
$\boldsymbol{\Delta S_P}$	Translation of point P
T	Draft of the floater
$\boldsymbol{\Delta\theta}$	Rigid body rotation
$\mathbf{V}$	Matrix of eigenvectors
WT	Wind Turbine
$\mathbf{X}$	Excitation vector
z_G	Vertical coordinate of the centre of gravity

1.2. Motivation

For a floating rigid body undergoing a general plane motion in 6 degrees of freedom (DOF), at a given instant, it is possible to define a point in space at which the velocity is zero [13]. In this paper, this point is referred to as the Instantaneous Centre of Rotation (ICR). As will be shown, such a point does not necessarily lie within the body, nor is it fixed in space, contrary to what may be commonly believed. Identification of such point is crucial as it can improve the understanding of the dynamic behaviour of FOWT, which, in turn, can lead to better motion reduction methods and may be leveraged to improve the design of these highly dynamic systems.[1]

Since the CR does not necessarily coincide with the centroid of the waterplane area [14] (except for the special case of very small rotations with no dynamic forces acting on the freely floating body), the side of the floater facing the incoming waves experiences different

---

[1] Note that identification of ICR is not strictly required to compute the responses with fully-coupled aero-hydro-servo-elastic nonlinear time domain dynamic solvers, in which case the physics of the problem (distributed loads) drive the ICR, and not vice versa. The knowledge of ICR is useful for lower-fidelity numerical models that make assumptions about the centre of rotation (CR), as well as to understand the FOWT coupled motion patterns.

amplitudes of vertical motion than the opposite side [15] - the pitch response is not symmetrical, even for a symmetrical structure. Acknowledgement of this may influence the design of the damping plates for the semi-submersible floating platforms, which could be optimised to take advantage of the load asymmetry. While the asymmetry would have much less pronounced effects in the case of the ballast-stabilised platforms, which tend to have small waterplane area and small second moment of waterplane area, knowing the vertical position of the pitch CR would be beneficial for the design optimisation of their mooring system. Placing the interface of the lines with the floater, i.e., fairleads, near the centre of rotation would limit the dynamic part of the motion that does not contribute to useful restoring. Likewise, the possible benefits for the dynamic power export cables' design are to be explored. Last but not least, manipulation of the vertical position of the CR through design modifications may help reduce the motions at the hub level, effectively reducing the undesired aerodynamic load variability and fatigue loads, as well as reducing human exposure to motion, improving the safety of the onsite maintenance operations.

Despite all the potential benefits, the identification of the ICR has received very little or no consideration in the floating offshore wind community. In fact, the majority of the literature focuses on static or quasi-static scenarios, with the assumption of small motions around an equilibrium position and a fixed CR. Although these assumptions allowed making significant progress in understanding the responses of FOWT and led to the development of useful analysis and design tools, the field still lacks an appreciation of the unsteady behaviour of these structures. The literature often refers to *the centre of rotation*: a single point (or axis) about which the system is assumed to rotate. While such a point can indeed be defined at a particular instant in time, for example, at an instant when the platform is in equilibrium, this gives no insight into the platform motion patterns during the motion. To the best of the author's knowledge, no methods to study and describe the highly complex time-dependent rotational motion of the floating offshore wind turbine platforms have been developed up to date.

1.3. Previous work

Among the earliest studies, Standing [16] determined the roll centre of a barge to enable the separation of sway and roll equations, challenging the assumption that CR aligns with the centre of gravity. Through (i) analytical derivation and (ii) experiments, the author showed that for a freely floating body: (i) if damping can be ignored, the centre of the roll can be assumed at the *centre of mass + added mass*; (ii) if damping is significant, the centre of the roll generally lies very close to that defined in (i), approaching it as the damping tends to zero. The author defined the *instantaneous roll centre* as the point which is instantaneously at rest as the vessel moves in waves, noting its erratic behaviour: "*this point tends to wander wildly, and in irregular waves can move from well above to well below the vessel*". Stewart and Ewers [17] tested a full-scale barge and observed near-infinite oscillations of the roll centre, explained by the simultaneously large sway velocity and very small roll angular velocity.[2] Regarding the offshore floating structures, Haslum and Faltinsen [18] investigated the CR in the coupled surge-pitch motion of a spar platform, considering two different vertical locations of the mooring attachment point. The CR was obtained as part of the solution to the special eigenvalue problem for free undamped oscillations, modified for the impact of the mooring system. A significant sensitivity of the CR to the oscillation frequency and fairlead location has been demonstrated; time dependency, however, could not be studied with the approach employed.

Most of the recent literature on the ICR of floating bodies focuses on FPSO vessels. Souza et al. [19] developed an experimental procedure to obtain the ICR in the roll free decay test. The authors obtained the

---

[2] The condition expected when a vessel follows long-period waves.

ICR by intersecting the perpendiculars to the velocity vectors measured at two distinct points in the floating body: this approach is, in fact, well established in the general kinematics theory [13], and will form the basis for the current investigation, as explained in Section 2. Fernandes et al. [14] built on that study by performing experiments in regular waves close to the roll natural period, supported by additional numerical calculations in the frequency domain. The authors showed that the ICR locus of an FPSO vessel is a straight line not coinciding with the line of symmetry of the vessel, dependent on the frequency of the waves. Costa et al. [20] tested the model in a range of regular head waves of different frequencies. Two position trackers allowed the calculation of the pitch angle by geometry and subsequent calculation of the ICR as the ratio between the displacement of a marker and the pitch angle. The mean ICR over the markers was considered to represent the intersection of the curves normal to the velocities at the markers, similar to [19]. An analytical expression for the locus of the ICR was derived, dependent on the motion amplitudes and phases in surge, heave, and pitch, showing good agreement with experimental results for some, but not all, of the frequencies. At very low frequencies, the behaviour similar to that of a pure translation was observed, with the ICR locus asymptotically tending to a horizontal line and to an infinite distance above the floating body. At very high frequencies, the locus tended to a vertical line and to an infinite distance below the floating body. In [21], the distributions of both the vertical and horizontal components of the ICR along the locus line were found to adhere to the Cauchy probability density function. In the latest article by Costa et al. [22], the investigation was extended to the consideration of oblique seas and 6 DOF motions. Once again, the ICR's dependence on the frequency of the regular waves has been demonstrated through a numerical approach (potential flow theory).

Note that the articles mentioned above focused on free-body motion, with the experiments set up to minimise the mooring system's influences. Up to the best knowledge of the authors, no study of ICR in irregular waves and more complex environmental conditions (combined wind and wave load) was performed up to date for any offshore floating platform.

In the realm of FOWT, there is increased recognition of the need to locate the centre of pitch rotation. The vertical separation of the CR and rotor notably affects the aerodynamic loads, impacting the relative velocity due to platform oscillations [23–25]. Wen et al. [24] studied the effect of the combined surge and pitch motion of a spar-supported WT on the effective rotor velocities, assuming the pitch centre to be constant in space and time; the exact position has not been reported. Tran et al. [26] and Liu et al. [27] studied the coupled dynamics of FOWT by the Computational Fluid Dynamics approaches. Tran et al. [26] assumed a fixed centre of rotation at 90 m below the hub centre, noticing, however, that for different foundation concepts, this assumption might not hold. Liu et al. [27] assumed the system rotated about an axis through the centre of mass. Kelberlau [28], on the other hand, assumed the CR of a semisubmersible floater to be located at the midpoint between the centre of gravity and the centre of buoyancy.

Eliassen [29] demonstrated the first attempt to investigate the centre of rotation of a FOWT without any presupposition about its location. Rather than assuming an arbitrary point, the z-coordinate of the centre of rotation has been calculated based on the mass, added mass, and stiffness properties through the ratio of two eigenmodes. Kaptan et al. [30] studied how wave frequency influences the CR of two different floating concepts. The authors assumed that a single point where the total horizontal motion (with contributions from the surge and pitch motions) is zero could be identified. Following the observation that the z coordinate of such a point would satisfy $\eta_1 + z\eta_5 = 0$,[3] the CR was obtained based on the ratio of the complex transfer

functions between the surge and pitch motions and the wave amplitude. Almost no dependence on the wave frequency for the spar platform and a significant, non-monotonic dependence for the semisubmersible platforms were indicated.

1.4. Scope of the current work

In this paper, the ICR of FOWT is studied by adopting a two-fold approach to ensure a fundamental understanding of the physics underpinning the phenomenon and its sensitivity to environmental conditions:

1. An analytical method at the surge, heave and pitch natural frequencies,
2. A hybrid method using the basic concepts of rigid-body kinematics and time-domain numerical analysis for a range of deterministic and stochastic environmental conditions.

The rest of the paper is organised as follows. The methodology is described in Sections 2.1–2.3, starting with the numerical (time domain) approach, followed by the analytical approach and case study definition. All results are presented and discussed in Section 3, and the paper is concluded in Section 4.

2. Methodology

2.1. Rigid body kinematics and time-domain analysis

When subjected to the head waves' load, a FOWT undergoes general plane motion, with components in the surge, heave, and pitch directions (assuming perfect symmetry in the x–y plane[4]). The centre of the pitch rotation depends on the distribution of forces acting on the body and its determination is, in general, nontrivial. It is possible to define a point (not necessarily within the body) that has zero velocity at a particular instant in time, that is, the ICR. Any other point in the body presents pure rotation about this point at that instant of time, i.e., follows a circular path around the ICR [13]. Therefore, the ICR must lie at the intersection of the perpendiculars to the velocities of two arbitrarily chosen points (A and B in Fig. 1(a)) through these points, assuming a rigid body. In the special case when the velocity vectors are parallel, and the line joining points A and B is perpendicular to the velocities, an alternative method is required. In that case, the ICR can be obtained through a direct proportion [13], as illustrated in Fig. 1(b). The vectors required for this calculation can be found by measuring the velocities in A and B, as obtained from the time-domain numerical simulations.

Note that the location of the ICR changes as the body moves, both in terms of the body-fixed and global inertial coordinate systems, and therefore, it only exists at a particular instant in time. The current investigation uses the concept of the space centrode, i.e. the locus of the positions of the instantaneous centre in space [13], to study how the ICR position changes in the global inertial coordinate system as a function of time.

The statistics of the ICR over the full analysis time are studied, including the mean, standard deviation, mode, and the Expected Value of the in-plane coordinates of the ICR (i.e., x and z coordinates). The mode (position of the peak of the distribution) gives a useful indication of the most often encountered values. However, in the cases where the ICR distributions are multimodal, the Expected Value is a more useful statistic. It is defined as the value that is the most likely result of the next repeated trial of a statistical experiment [31] and uses the probabilities of possible outcomes as weights in the process of finding the weighted average of the data in a data set. In this study, it is adapted

---

[3] That is, a combination of pure translation η_1 and the translation due to the rotation η_5 of the system's origin around the centre of rotation, should be equal to zero.

[4] The coordinate system is defined in Section 2.3 and in Fig. 2.

(a) General case - misaligned nodes
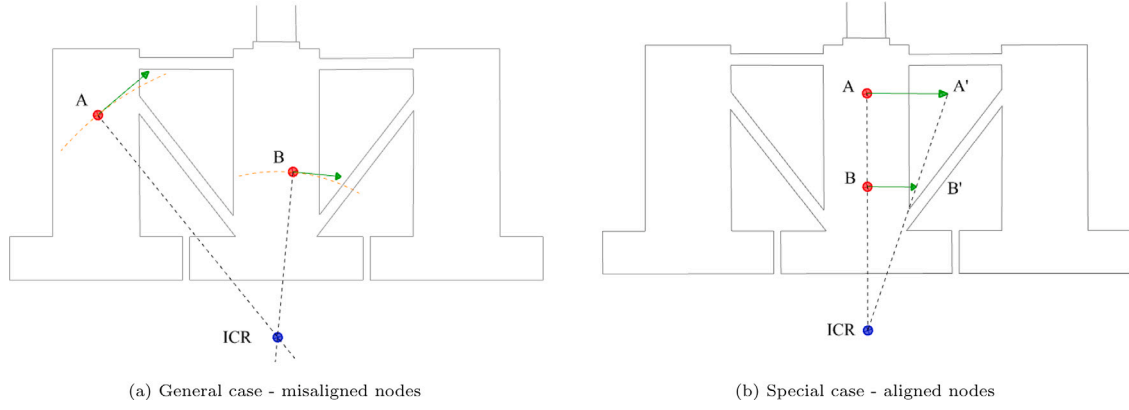
(b) Special case - aligned nodes

Fig. 1. Construction of the Instantaneous Centre of Rotation using two misaligned (a) and aligned (b) points on the floating body.

to find the average ICR coordinates weighted with the frequency of occurrence in the time signal recorded over ten pitch periods, sampled at 0.0125s. Additionally, time histories and histograms of the ICR and rigid motions are presented to complete the picture.

This study uses OpenFAST - a state-of-the-art, extensively validated nonlinear aero-hydro-servo-elastic coupled time-domain model of dynamics [32]. The focus is on modelling the hydrodynamic and mooring loads. Hence, the influences from the aerodynamics and control system are ignored. Likewise, the analysis assumes the floater is a rigid body. Therefore, the elastic dynamics are not modelled. Frequency-to-time-domain transforms based on the potential coefficients obtained from the Boundary Element Method code WAMIT [33] are used to model the 1st-order hydrodynamics. Viscous loads are computed from Morison's theory. The nonlinear mooring loads are calculated using a quasi-static model MAP++ [34,35]. The code calculates steady-state forces on the mooring lines' segments, including the effects of the seabed contact (kinetic friction force calculated as the product of a kinetic friction coefficient and the seabed contact normal force). The catenary line profile and effective forces are computed based on the distributed line mass, strain, and elasticity, for a line suspended in static equilibrium (hence *quasi-static*). Forces arising from the inertia, viscous drag, internal damping, bending and torsion are all ignored.

2.2. Analytical model — eigenproblem solution

The method presented here follows that previously introduced in [20,22,36]. The motion of a generic point A of the floating body in 6 DOF can be represented as a combination of the point's translation with respect to a generic reference point C ($\Delta\mathbf{S_C}$), and its rotation by a small angle around the same reference point ($\Delta\theta$). By definition, this transformation can be considered a pure rotation about the ICR. Therefore:

$$\Delta\mathbf{S_A} = \Delta\mathbf{S_C} + \Delta\theta \times \mathbf{r_{A,C}} = \Delta\theta \times \mathbf{r_{A,ICR}} \tag{1}$$

Similarly, the motion of point C (moving along with the rigid body) can be seen as a pure rotation about the ICR, which can be written as:

$$\Delta\mathbf{S_C} = \Delta\theta \times \mathbf{r_{C,ICR}} \tag{2}$$

Alternatively:

$$\eta_1\hat{\imath} + \eta_2\hat{\jmath} + \eta_3\hat{\mathbf{k}} = (\eta_4\hat{\imath} + \eta_5\hat{\jmath} + \eta_6\hat{\mathbf{k}}) \times (x_{C,ICR}\hat{\imath} + y_{C,ICR}\hat{\jmath} + z_{C,ICR}\hat{\mathbf{k}}) \tag{3}$$

This yields a set of three equations:

$$\eta_1 = z_{C,ICR}\,\eta_5 - y_{C,ICR}\,\eta_6 \tag{4}$$

$$\eta_2 = x_{C,ICR}\,\eta_6 - z_{C,ICR}\,\eta_4 \tag{5}$$

$$\eta_3 = y_{C,ICR}\,\eta_4 - x_{C,ICR}\,\eta_5 \tag{6}$$

For the case of the head waves, and considering a body symmetrical with respect to the x–y plane, the motions in sway, roll and yaw (η_2, η_4, η_6) are all zero, hence the system can be reduced to:

$$\eta_1 = z_{ICR,C}\,\eta_5 \tag{7}$$

$$\eta_3 = -x_{ICR,C}\,\eta_5 \tag{8}$$

Note that, in general, the motions in the $x - z$ plane, which are necessary to solve this system, are functions of wave frequency and time, as given by:

$$[\mathbf{M} + \mathbf{A}(\omega)]\ddot{\boldsymbol{\eta}}(t) + \mathbf{C}\boldsymbol{\eta}(t) = \mathbf{X}(t, \omega, \theta) \tag{9}$$

where $\mathbf{M}$ is the mass matrix, $\mathbf{A}(\omega)$ is the frequency-dependent hydrodynamic added mass matrix, $\mathbf{C}$ is the stiffness matrix, and $\mathbf{X}(t, \omega, \theta)$ is the frequency and direction-dependent excitation vector (note that damping is ignored here).

At the surge, heave and pitch natural frequencies, however, the position of the centre of rotation of a FOWT can be approximated by solving the eigenvalue problem, formulated in Eq. (10):

$$(\boldsymbol{\omega}, \mathbf{V}) = eig([\mathbf{M} + \mathbf{A}]^{-1}\mathbf{C}) \tag{10}$$

$$\boldsymbol{\omega} = [\omega_1, \omega_3, \omega_5] \tag{11}$$

$$\mathbf{V} = [\mathbf{V_1}, \mathbf{V_3}, \mathbf{V_5}] \tag{12}$$

$$\mathbf{V_i} = [V_{i,1}, V_{i,3}, V_{i,5}] \tag{13}$$

where $\boldsymbol{\omega}$ is the vector of eigenvalues and $\mathbf{V}$ is the matrix of the corresponding eigenvectors. Then, Eqs. (7) and (8) are rearranged to calculate the coordinates of the Initial Centre of Rotation for the ith mode:

$$x_{ICR,C}\Big|_{\omega_i} = -V_{i,3}/V_{i,5} \tag{14}$$

$$z_{ICR,C}\Big|_{\omega_i} = V_{i,1}/V_{i,5} \tag{15}$$

The eigenvalue problem formulation allows for a simplified calculation without running numerical simulations — an approach that can be useful when the information about the system is very limited (e.g., at very early design stages), providing a fundamental understanding of the system's behaviour.

Having simplified the problem to a two-dimensional problem in the vertical plane (i.e., considering the surge, heave and pitch motions alone), and assuming mass distribution perfectly symmetrical about the $x - z$ plane, the mass matrix of size 3×3 is:

$$\mathbf{M} = \begin{bmatrix} m & 0 & mz_G \\ 0 & m & 0 \\ mz_G & 0 & I_{yy} \end{bmatrix} \tag{16}$$

where m is the total mass of the system, z_G is the z coordinate of the centre of gravity of the system, and I_{yy} is the second moment of inertia about the axis parallel to y-axis passing through the centre of gravity.

Assuming that the flow at each section of the floater is two-dimensional, the added mass matrix:

$$\mathbf{A} = \begin{bmatrix} A_{11} & 0 & A_{15} \\ 0 & A_{33} & 0 \\ A_{51} & 0 & A_{55} \end{bmatrix} \tag{17}$$

can be defined analytically, based on strip theory [37,38]. The infinite-frequency added mass components can be obtained by integration over the draft T of the floating structure [39][5]:

$$A_{11} = \int_{-T}^{0} m_A \, dz \tag{18}$$

$$A_{15} = A_{51} = -\int_{-T}^{0} z m_A \, dz \tag{19}$$

$$A_{55} = \int_{-T}^{0} z^2 m_A \, dz \tag{20}$$

The 2-dimensional added mass of the ith section of the floating cylinder is given by $m_A = \rho C_A A_i$, with ρ being the water density, C_A - analytical deep water added mass coefficient, equal to 1.0 for a circular section [40], A_i - reference area given by πR_i^2, with R_i being the radius of the section.[6] The heave added mass A_{33} was obtained based on the integration of the sectional added mass of vertical sections through the cylinder with $C_A = 2.23$ and $A_i = \pi a_i^2$, where a_i is the half-width of the ith vertical section [40] (the sections were assumed to be rectangular, therefore ignoring the tapered segment immediately under the free surface).

Restoring matrix includes the contributions from the hydrostatic, gravitational, and mooring stiffness:

$$\mathbf{C} = \begin{bmatrix} Cm_{1,1} & 0 & Cm_{1,5} \\ 0 & \rho g A_{WP} + Cm_{3,3} & 0 \\ Cm_{5,1} & 0 & \rho g I_{WL} + mg(z_B - z_G) + Cm_{5,5} \end{bmatrix} \tag{21}$$

Note that both the floating structure and the mooring configuration are assumed to be symmetric about the x-axis, and the response is assumed to be confined to the $x-z$-plane. The heave-pitch coupling is assumed to be negligible. The mooring stiffness can be obtained based on published data about the system [41].

No damping is assumed for this analytical calculation. Also, note that only the centre of rotation at the natural frequencies can be analysed by this method. Moreover, since the matrices required by this method are taken at the initial undisplaced position of the platform, the centre of rotation found this way will be termed *Initial Centre of Rotation*.

2.3. Case description

The results presented here relate to the case of the OC3 Hywind spar platform with a catenary mooring system, as defined in [41], and the NREL 5MW reference wind turbine, as defined in [42]. The main characteristics are summarised in Table 1. The origin of the coordinate system is located at the centre of flotation, i.e., at the centroid of the initial (undisturbed) waterplane area, as indicated in Fig. 2. The positive x-axis is in the direction of the incoming waves, and the positive z-axis is upward. The time domain simulations are carried out in regular and irregular waves for a range of wave periods and heights outlined in Table 2. The JONSWAP frequency spectrum is used to generate irregular waves, as recommended by the IEC 61400-3 Annex B [43] and shown in Fig. 3.

---

[5] The formulations from [39] were modified by discarding the forward speed components.

[6] Note that this approach is not limited to cylinders; it can be applied to structures of any shape, as long as the sectional added mass coefficients can

Table 1
OC3 Hywind spar characteristics.
Source: Retrieved from [42].

Item	Value	Unit
Water displacement	$8.23 \cdot 10^6$	kg
Platform mass	$7.47 \cdot 10^6$	kg
Platform draft	120.0	m
Radius to anchors from centreline	853.87	m
Platform vertical centre of gravity	-89.92	m
Natural frequency: surge and sway	0.050	rad/s
Natural frequency: heave	0.201	rad/s
Natural frequency: roll and pitch	0.214	rad/s

Table 2
Case study definition — wave conditions.

Waves type (–)	(Peak) period (s)	(Significant) wave height (m)
Regular	10.47 – 125.66	2.0, 4.0, 8.0
Irregular	10.47, 31.25, 125.66	2.0, 4.0, 8.0

Table 3
Initial centre of rotation coordinates at three eigenvalues, as obtained by the analytical method.

Eigenvalue (rad/s)	Initial x_{ICR} (m)	Initial z_{ICR} (m)
0.05	$-\infty$	$-\infty$
0.20	$-\infty$	∞
0.21	0.0	0.0

3. Results and discussion

3.1. Initial Centre of Rotation — analytical approach

The method described in Section 2.2 was followed to find the coordinates of the centre of rotation at the instant when the platform is in equilibrium, i.e., using the mass, added mass, and stiffness matrices derived in that position, for the surge-heave-pitch coupled motion, as reported in Eqs. (22)–(24). Note that the effect of damping is neglected in this analysis.

$$\mathbf{M} = \begin{bmatrix} 8.07E+06 & 0 & -6.29E+08 \\ 0 & 8.07E+06 & 0 \\ -6.29E+08 & 0 & 6.80E+10 \end{bmatrix} [\text{kg}] \tag{22}$$

$$\mathbf{A} = \begin{bmatrix} 8.23E+06 & 0 & -5.10E+08 \\ 0 & 2.49E+05 & 0 \\ -5.10E+08 & 0 & 4.09E+10 \end{bmatrix} [\text{kg}] \tag{23}$$

$$\mathbf{C} = \begin{bmatrix} 4.12E+04 & 0 & -2.82E+06 \\ 0 & 3.34E+05 & 0 \\ -2.82E+06 & 0 & 1.48E+09 \end{bmatrix} [\text{N/m, Nm/rad}] \tag{24}$$

The calculated values of the Initial Centre of Rotation are reported in Table 3. At the pitch natural frequency (0.21 rad/s), the point calculated by the analytical method perfectly coincides with the centre of floatation, which agrees with what is commonly agreed in the literature on hydrostatics of floating bodies [44,45]. At the surge and heave natural frequencies, on the other hand, the Initial Centre of Rotation was calculated to be at an infinite distance from the origin, which was expected for the translational modes (rotation at an infinite radius is equivalent to a pure translation or no rotation).

3.2. Centre of rotation in forced motion: time domain approach

The method described in 2.1 was applied to study the time history and statistics of the ICR coordinates during the motion of the moored

---

be obtained, for instance through a potential flow solution. Here, we applied the most fundamental solution.
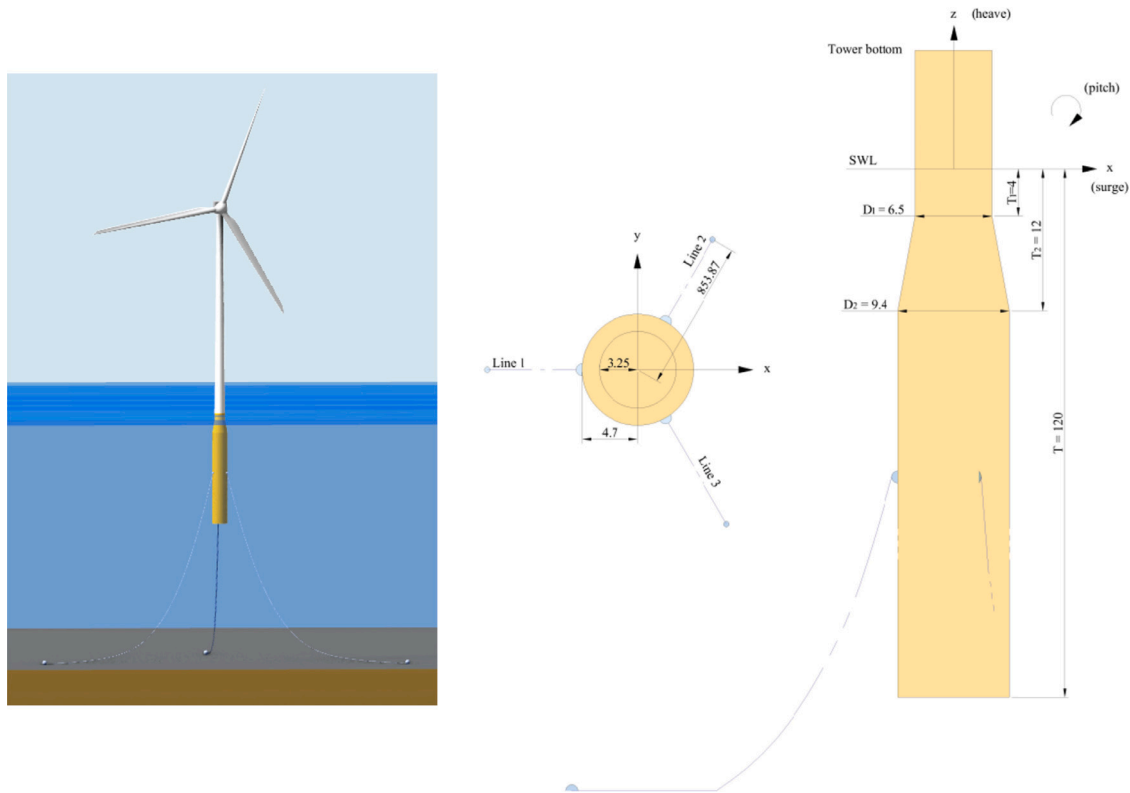
Fig. 2. A system representative of the OC3 Hywind spar. Dimensions in meters; not true to scale.
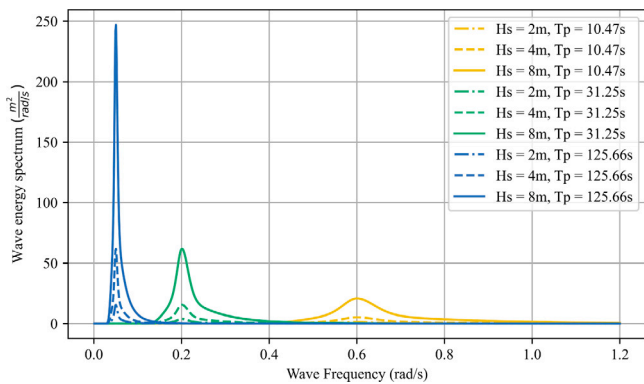

Fig. 3. Wave energy spectra for 9 sea conditions (JONSWAP).

platform in regular and irregular waves. The results of the two series of tests will be presented in turn.

3.2.1. Regular waves

The simulations were carried out in regular waves of three different heights (2 m, 4 m, and 8 m), at periods ranging from 10.47 s to 125.66 s. Fig. 4 presents the time history of the horizontal and vertical coordinates of the ICR (x_{ICR} and z_{ICR}) during the platform's motion in 2 m waves of frequency equal to the natural pitch frequency (0.2 rad/s), plotted together with the pitch motion signal. The last 10 pitch periods are shown. Both x_{ICR} and z_{ICR} present periodic behaviour with tangent-like and parabolic shapes, which are the consequence of the pitch motion changing direction twice every cycle. At instances when the pitch velocity is zero (i.e., pitch displacement reaches maximum or minimum), the ICR becomes infinity. The physical interpretation can be made by examining a single pitch period, as displayed in

Fig. 5. Four phases of the pitch motion can be distinguished, each with characteristic ICR behaviour:

- Phase 1: as the pitch angle increases from zero to maximum, the x-coordinate of the ICR decreases from 19.5 m to minus infinity. The infinite x_{ICR} at the pitch motion peak corresponds to an instantaneous lack of rotation or a pure translation. As mentioned before, this is to be expected as, at this point, the pitch motion changes direction, hence the platform momentarily becomes static. z_{ICR} presents a similar behaviour, except, it increases to plus infinity at the end of the phase. A discontinuity is seen in both coordinates shortly after half of the phase — as will be shown later in this section, this is the effect of the mooring lines restraining the motion of the platform.
- Phase 2: as the pitch angle decreases from maximum to zero, the x-coordinate of the ICR decreases from plus infinity to a finite value of 22.2 m. z_{ICR} follows an opposite trend, increasing from minus infinity to a negative value of -61.9 m.
- Phase 3: as the platform pitches towards the opposite direction, x_{ICR} repeats the same pattern as in phase 1. z_{ICR} increases to plus infinity, with a discontinuity shortly after the half of the phase.
- Phase 4: as the platform returns to its initial position, x_{ICR} decreases back to 19.5 m, and z_{ICR} increases back to -61.9 m. Note the anti-symmetry of the x_{ICR} plot.

Both coordinates span infinite ranges. Although the above analysis aids the understanding of the dynamics of the platform pitch motion, it does not allow for the identification of a point of minimum additional translation due to the rotation during general motion, which is of practical interest. For this reason, the statistics of x_{ICR} and z_{ICR} are examined next, as listed in Table 4.

The positive value of mode of x_{ICR} indicates motion asymmetry — the ICR concentrates 27.98 m aft of the Centre of Flotation (i.e., origin of the assumed coordinate system). The consequence of this is that the side of the floater facing the incoming waves experiences a
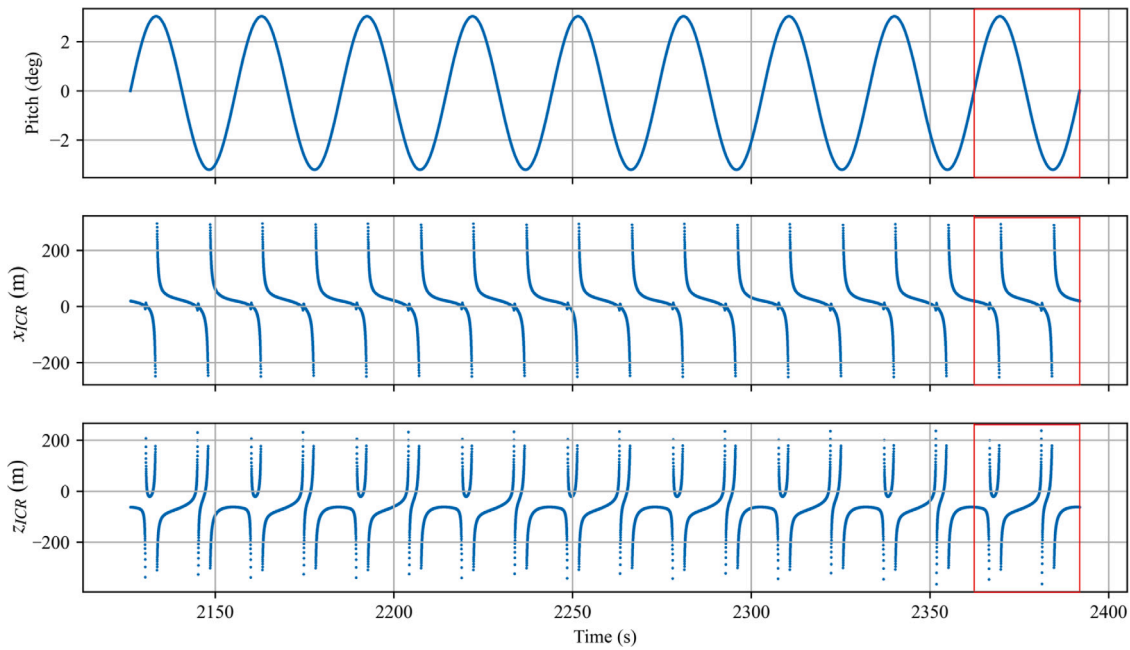
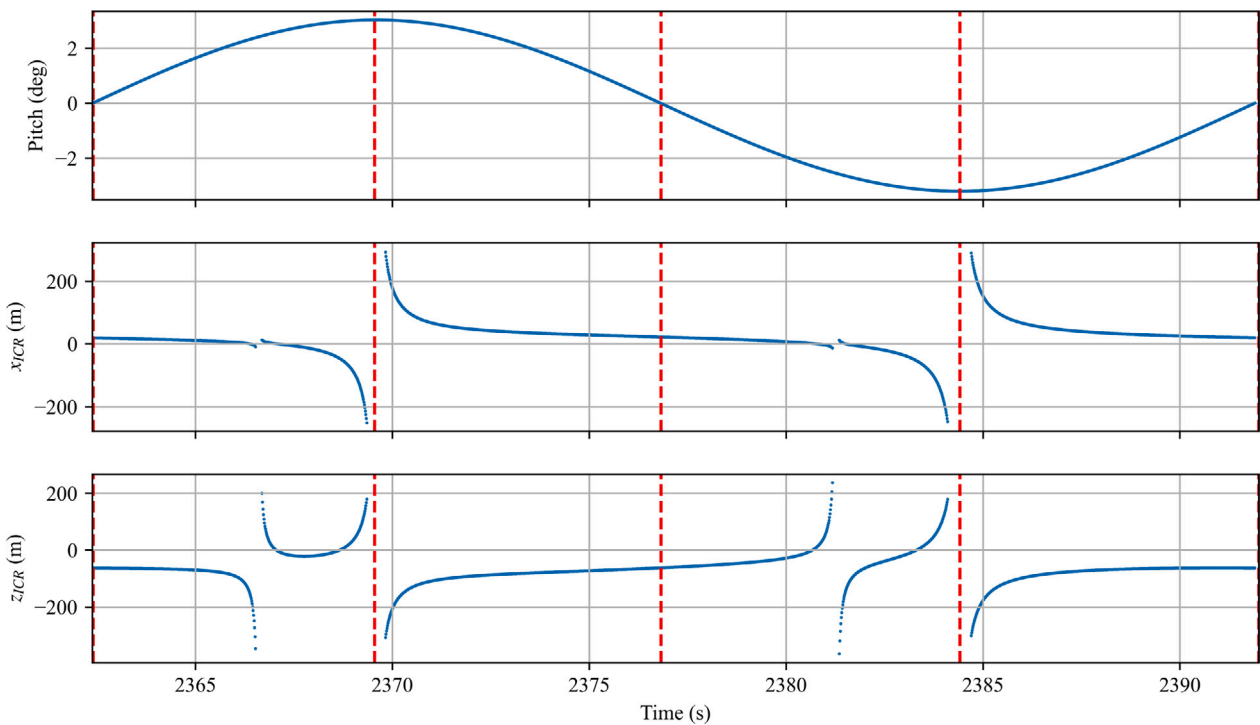**Fig. 4.** ICR time history in pitch natural frequency regular waves motion for 10 pitch periods.

Fig. 5. ICR time history in pitch natural frequency regular waves motion for 1 pitch period, derived from Fig. 4.

Table 4
Statistics of the ICR components based on the last 10 pitch periods, for the pitch natural frequency.

	x_{ICR} (m)	z_{ICR} (m)
Mean	30.73	−101.35
Mode	27.98	−102.38
Expected Value	20.61	−62.27
Standard deviation	3019.99	264.24

higher amplitude of motion. The mode of z_{ICR} (−102.38 m) is at a depth not coinciding with any of the commonly considered characteristic points (i.e., the centre of flotation, buoyancy, gravity and the fairlead attachment point). The large vertical distance from the most often encountered centre of rotation from the hub impacts the velocities and accelerations encountered at the hub level. Both coordinates have a high standard deviation, indicating that the values are spread out over a wide range. While x_{ICR} distribution is almost perfectly symmetric around the mean, z_{ICR} is skewed away from the mean. This is a consequence of the fact the z_{ICR} follows a bi-modal distribution, as demonstrated in Fig. 6, where the space centrode of ICR is plotted
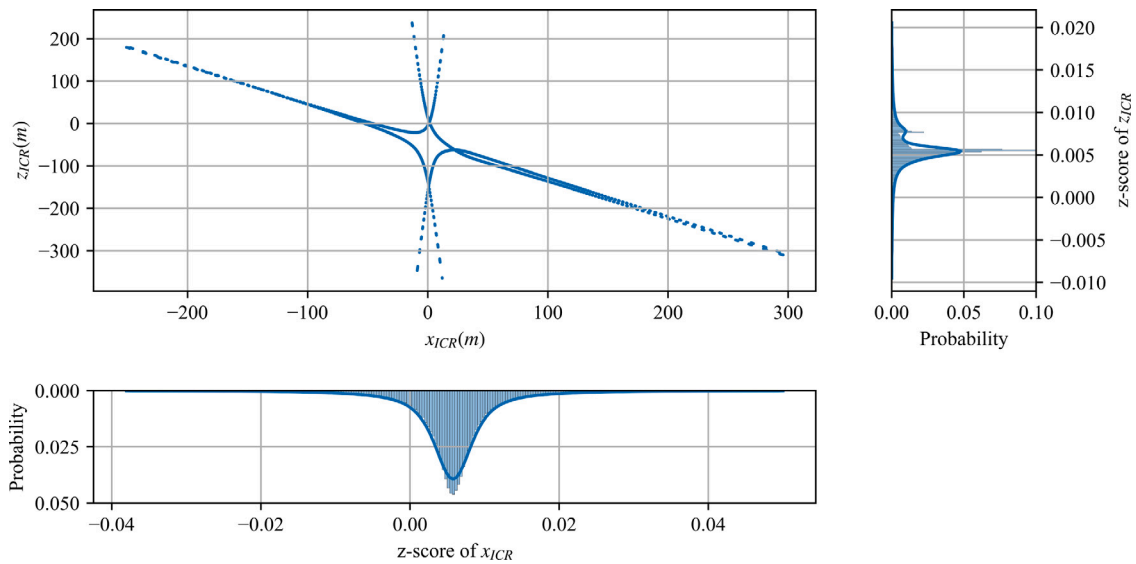
Fig. 6. ICR space centrode with probability distributions of the x and z coordinates.
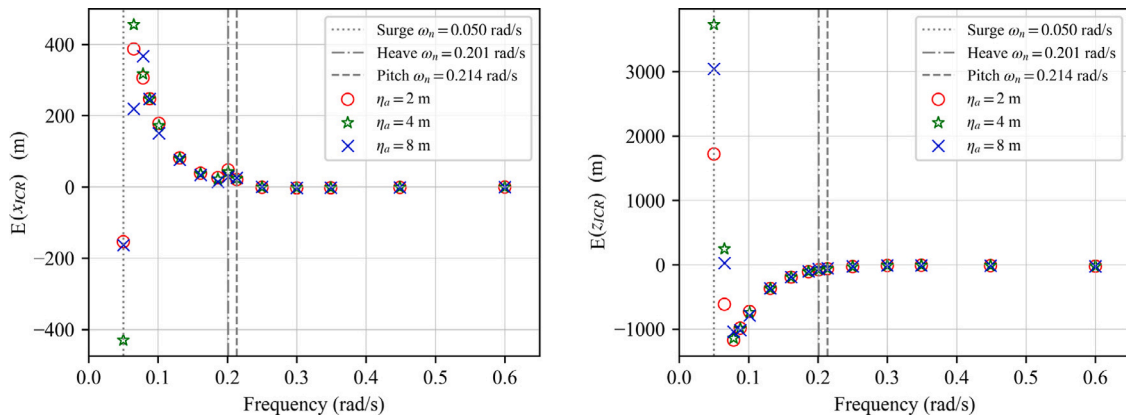

Fig. 7. The Expected Value of ICR as a function of frequency for different wave heights.

together with the probability distributions. The space centrode of ICR consists of four curves, with the points concentrated near the centre of the plot. This shows that, at this frequency, the rotational behaviour of a FOWT is significantly more complex than that of FPSO vessels, the centrodes of which have been reported to be straight lines in multiple references, including [21]. Hence, unlike for FPSO, derivation of an analytical model for the ICR centrode would be very challenging.

Lastly, the dependence of the ICR coordinates on the frequency and height of the incoming regular waves was studied. A clear dependence of both ICR coordinates on the frequency of the waves has been observed. $E(x_{ICR})$ peaks at a frequency slightly higher than the surge natural frequency, following a downward trend thereafter (Fig. 7). An opposite tendency is observed for $E(z_{ICR})$. In the low-frequency limit, x_{ICR} and z_{ICR} tend to minus and plus infinity, respectively, which corresponds to a pure translation. The value of ICR increasing with the frequency decreasing is consistent with the behaviour observed previously in [17], where the large ICR values were associated with the condition of the long waves, whereby a floating body follows the profile of the sea surface. In the high-frequency limit, both $E(x_{ICR})$ and $E(z_{ICR})$ tend to zero (i.e., the centre of floatation). At the pitch natural frequency (0.214 rad/s), $E(z_{ICR})$ peaks slightly due to the resonance between the rigid DOF and the oscillatory wave load, achieving values

of 20.7 m to 25.4 m and −62.2 m to −53.7 m, respectively, depending on the wave amplitude. Note that these values do not coincide with either the centre of floatation/gravity or the mooring attachment point. Divergence from the values obtained by the analytical approach (*Initial Centre of Rotation*), is also observed (recall the result of the analytical approach: $x_{ICR} = z_{ICR} = 0.0$ m). See Figs. 15 and 16 in Appendix A for a comparison of the time series of ICR coordinates at different frequencies.

As can be seen in Fig. 7, the Expected Value of both coordinates present significant sensitivity to the wave height at low frequencies and almost no sensitivity to the height at the frequencies higher than the pitch natural frequency. This characteristic behaviour at the low frequencies can, among other factors, be attributed to:

- mooring loads, nonlinear in platform offset: a catenary mooring system provides the station-keeping ability in the function of the weight of the suspended line length: when the platform is displaced away from the equilibrium position, a portion of the line resting on the seabed is lifted, increasing the length of the freely-hanging chain and changing the angle of the lines, which nonlinearly affects the tension in the lines and the load on the
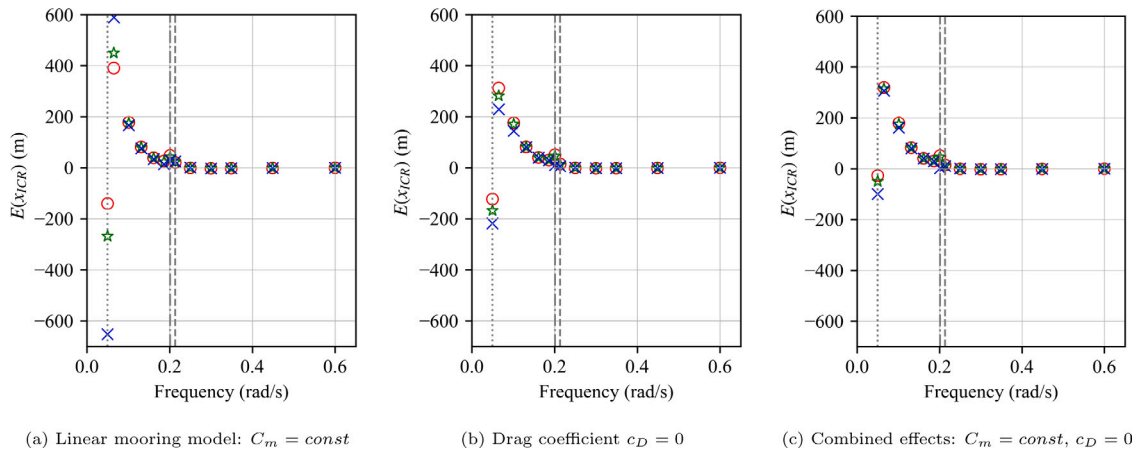
| (a) Linear mooring model: $C_m = const$ | (b) Drag coefficient $c_D = 0$ | (c) Combined effects: $C_m = const, c_D = 0$ |

Fig. 8. Impact of nonlinear effects on $E(x_{ICR})$.

floating platform [46].[7] The changes in mooring stiffness due to the platform offsets impact the low-frequency surge motions [47, 48];

- viscous drag, nonlinear in wave amplitude: the viscous drag depends on the square of the relative velocity, i.e., the sum of the water particle velocity and the platform motion velocity [49], dependent on the wave height. The response of the FOWT near the resonant frequency (surge natural frequency) is highly dependent on the viscous loading on the platform [50,51].

Therefore, to explain the low-frequency discrepancies, the Expected Value has been recalculated modifying the underlying physical model to exclude the two nonlinear effects. The nonlinear mooring loads were eliminated by replacing the quasi-static mooring model with a linearised one (fixed stiffness matrix obtained at the undisplaced platform position). The nonlinear viscous loads were eliminated by setting the viscous drag coefficient within OpenFAST's strip theory approach to zero.

As presented in Figs. 8 and 9, both nonlinear effects (mooring and viscous loads) had a significant effect on the sensitivity of ICR to the wave height. Removing the viscous drag from the hydrodynamic model resulted in a significant reduction of the discrepancies in $E(x_{ICR})$ at all frequencies. Replacing the quasi-static mooring model with a linear one led to the reduction of the discrepancies in the $E(z_{ICR})$ at all but the lowest two frequencies considered. The two effects combined in such a way that the sensitivity of the ICR to wave height was greatly lowered (Figs. 8(c) and 9(c)).

The part of the mooring load linear in platform displacement was also found to contribute to the observed relationship between the ICR and wave height. Fig. 10 presents $E(x_{ICR})$ and $E(z_{ICR})$ as functions of wave frequency for different wave heights, obtained for an unmoored structure. A significant reduction of discrepancies at low frequencies can be seen, as compared to the standard systems' results (Fig. 7). Additionally, when the mooring load was removed from the model, both coordinates of ICR at 0.05 rad/s changed their signs, making the $x_{ICR}(\omega)$ and $z_{ICR}(\omega)$ curves monotonic. One more time, a significant impact of the mooring system on the dynamic behaviour of FOWT in low-frequency waves has been revealed.

Since the ICR is computed based on velocity vectors, its sensitivity to the wave height primarily stems from the sensitivity of the motion velocity to the wave height. Indeed, Fig. 11(b) demonstrates

the highly nonlinear relationship between the wave height and the platform motion velocity (measured at the system's origin), but only in the low-frequency case — this is not seen in the higher frequency (10 s) case (Fig. 11(a)).

The complex motion behaviour at the low frequency (e.i., in long waves) is partly due to the effect the moorings have on the system. In the coupled 6 DOF motion, due to large surge offsets, the mooring loads lead to the distortion of the heave and pitch motion patterns, as can be observed in Fig. 12(a). The linear part of the mooring load causes the so-called *hard clipping*[8]: while the pitch displacement of a freely floating (unmoored) platform in regular waves is purely sinusoidal at the fundamental frequency (here, wave frequency) (Fig. 12(a)), the linear mooring load restrains the platform's motion, flattening out the peaks of the signal. Hard clipping introduces odd harmonics (odd integral multiples of the wave frequency), which was also observed in the FFT analysis (Fig. 12(b)). The nonlinear mooring load, on the other hand, leads to saturation of the pitch motion, or the so-called *soft clipping*: when the surge or pitch amplitude approaches a certain limit (governed by the mooring tension), the curvature of the peaks of the pitch signal changes (Fig. 12(a)). Saturation introduces both odd and even harmonics at higher frequencies, as demonstrated in Fig. 12(b). The strength of these two effects is increasing with the wave height increasing, due to the increasing motion amplitude. In fact, the root cause of these phenomena is the large surge offset in low-frequency or long waves: eliminating the surge-pitch coupling[9] suppresses the higher harmonics, as depicted in Fig. 17 in Appendix B.

Note that the observed nonlinear relationship between the wave height and platform displacement and velocity at low frequencies also contributes to the effect of the viscous drag on the ICR presented before in Fig. 9(b).

3.2.2. Irregular waves

The study of the ICR of FOWT subjected to regular wave loading provided a good basis for the investigation of its behaviour in irregular waves, being one step closer to a real operational scenario which is of practical interest. To this end, the JONSWAP spectrum has been used to generate sea states of three different peak periods and three different significant wave heights, as per Table 2. For each condition, 30

---

[7] Note that this is true for the lines opposite to the direction of the platform movement; the opposite is true for the other lines.

[8] Clipping is a term primarily used in digital signal processing for a form of distortion that limits a signal once it exceeds a threshold [52,53] - the concept often used in audio and optical systems engineering.

[9] Achieved in OpenFAST by disabling all rigid body translational and rotational DOF except for the pitch rotation.
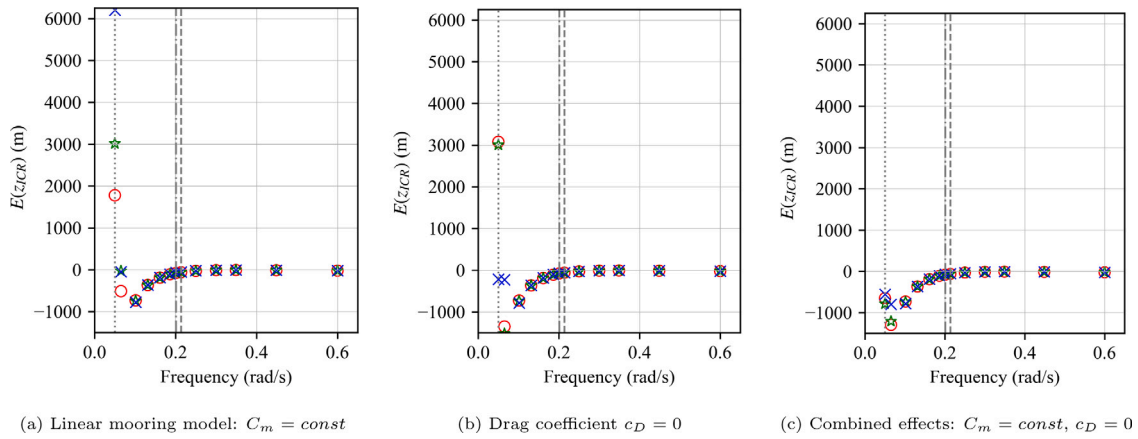
(a) Linear mooring model: $C_m = const$ (b) Drag coefficient $c_D = 0$ (c) Combined effects: $C_m = const$, $c_D = 0$

Fig. 9. Impact of nonlinear effects on $E(z_{ICR})$.
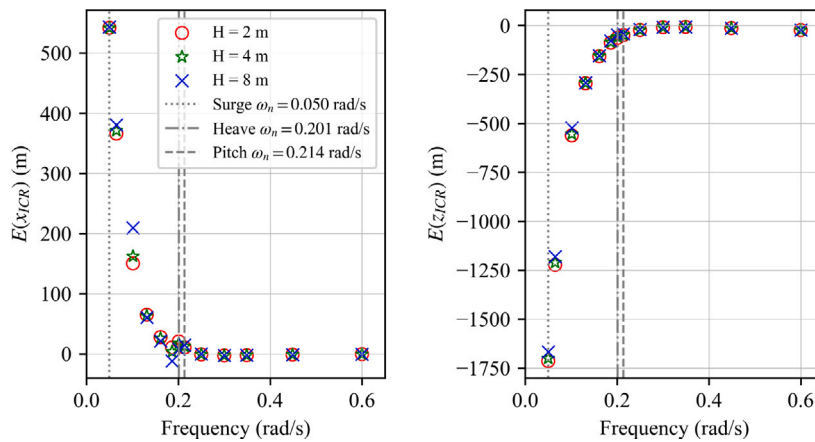

Fig. 10. Expected Value of ICR as a function of frequency for different wave heights H, obtained for an unmoored system. The surge, heave, and pitch natural frequencies are marked with vertical lines for reference.

random realisations were computed,[10] each including 3600 s of signal, sampled at 0.0125s. $E(x_{ICR})$ and $E(z_{ICR})$ were computed for each random realisation, and then the distributions over the 30 realisations were studied, as shown in Figs. 13 and 14. Similarly to the regular waves test, the focus was on the sensitivity of $E(x_{ICR})$ and $E(z_{ICR})$ to wave frequency (peak period in this case), and to the wave height (or, significant wave height).

$E(x_{ICR})$ generally decreases, and $E(x_{ICR})$ increases with frequency increasing, for all wave heights studied. This behaviour is consistent with that observed in the regular waves test, except for the lowest frequency (0.05 rad/s), where the regular and irregular waves loading resulted in opposite sign $E(x_{ICR})$ and $E(z_{ICR})$.

No statistically significant dependence of ICR on wave height was observed. As can be seen in Figs. 13 and 14, for any frequency, the ranges of the Expected Value of ICR are overlapping, as also confirmed by the Student's t-test.[11] As shown in Section 3.2.1, monochromatic low-frequency waves excite nonlinear hydrodynamic and mooring loads, which highly affect the rotational behaviour of the platform, increasing the sensitivity of the ICR to wave height. However, since an irregular sea state is composed of waves of various frequencies, these nonlinear effects are alleviated by the effect of higher frequency waves, which reduce that sensitivity.

---

[10] The number of random realisations was dictated by the number of samples required to perform the t-test, to study the statistical significance of the trends observed.

[11] Two-tail test, $\alpha = 0.05$, $t_{critical} = 2.042$, $t_{value} \in [0, 0.722]$.

4. Conclusions

This paper investigates the Instantaneous Centre of Rotation (ICR) of Floating Offshore Wind Turbines (FOWT). A two-fold approach was developed: (i) an analytical solution for the rigid body motion natural frequencies' centre of rotation (*Initial Centre of Rotation*); (ii) time-domain analyses in regular and irregular waves, to study the time-dependent behaviour of the ICR, and to establish its sensitivity to the wave frequency and height.

The results demonstrate that FOWT rotates about a point that is not fixed in time or space, necessitating the use of the term *Instantaneous Centre of Rotation*. The frequently used terms *Centre of Rotation/Pitch Centre* imply the existence of a single point fixed in time and space and, as such, should be avoided. The coordinates of the ICR span infinite ranges but tend to concentrate around finite locations. Statistically, the mean and mode of the ICR distributions generally differ from zero, indicating motion asymmetry. Specifically, the side of the floater facing the incoming waves experiences greater motion amplitude. The x coordinate of ICR follows a symmetrical unimodal distribution, while the z coordinate presents a multimodal distribution with significant skew.

In regular waves, the Expected Value of ICR depends on the wave frequency but is insensitive to wave amplitude, except for the lowest frequency case, primarily due to the mooring loads, both linear and nonlinear in platform offset, and viscous loads, nonlinear in wave amplitude. The mechanism leading to this relationship was identified: large surge offsets of the platform in long (low-frequency) waves lead to increased mooring loads, which, towards the end of each half of
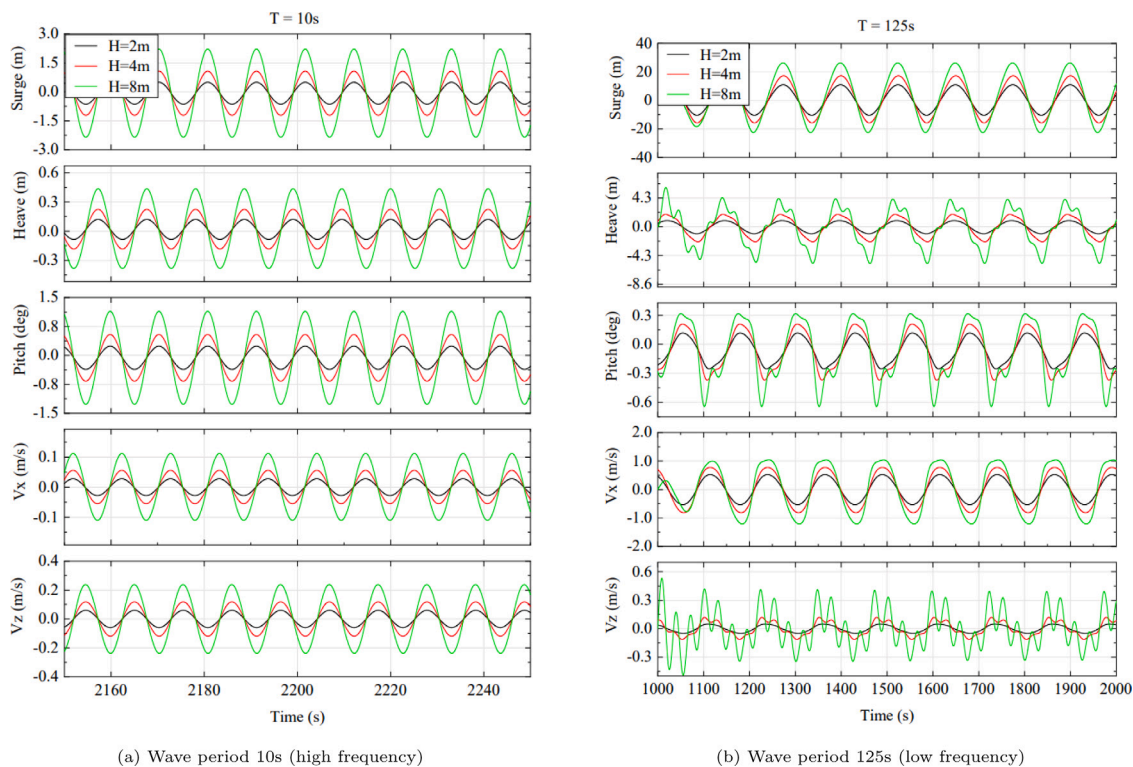
(a) Wave period 10s (high frequency)

(b) Wave period 125s (low frequency)

Fig. 11. Comparison of the surge and heave displacement and velocity time histories for two different wave frequencies.

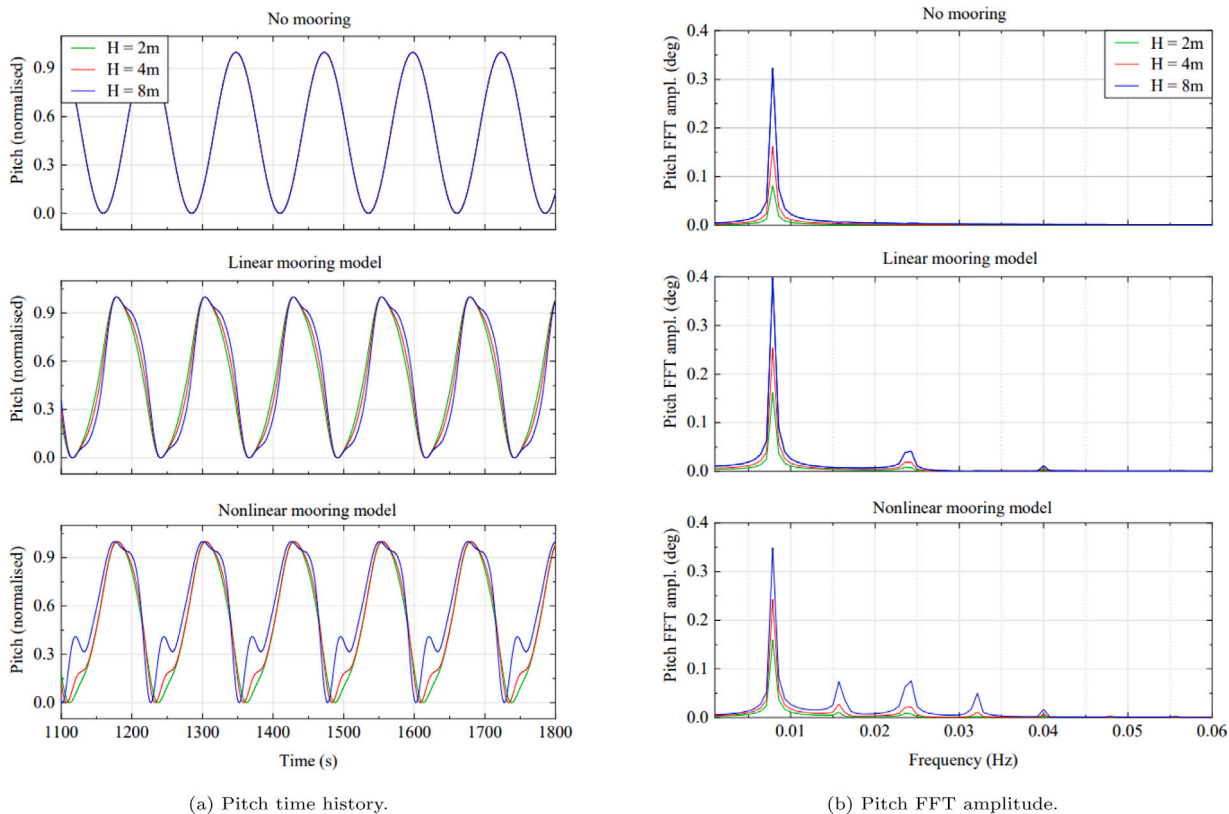(a) Pitch time history.

(b) Pitch FFT amplitude.

Fig. 12. The time history and FFT plots of the pitch motion obtained with different dynamic models.
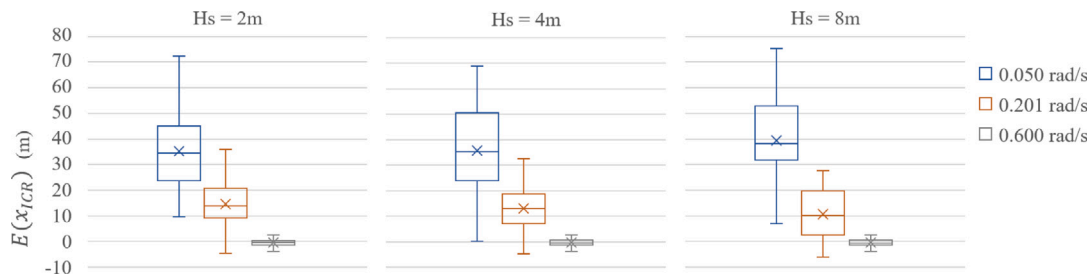
Fig. 13. $E(x_{ICR})$ in irregular waves, for three frequencies and three wave heights. Box plots based on 30 random realisations.
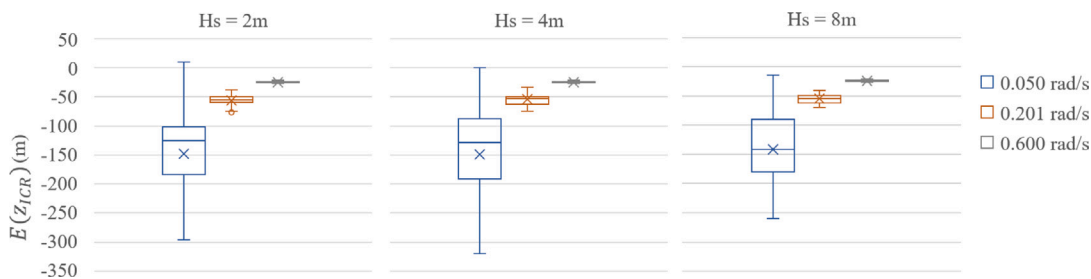

Fig. 14. $E(z_{ICR})$ in irregular waves, for three frequencies and three wave heights. Box plots based on 30 random realisations.

the surge cycle, affect the heave and pitch displacements and velocities introducing higher harmonics to these responses. Through this surge-heave-pitch coupling, the vertical velocities become highly nonlinear in wave height, resulting in a highly nonlinear ICR. This distortion of the heave and pitch motion patterns can be attributed to two effects: (i) hard clipping (flattening out the peaks of the signal), which introduces odd harmonics, (ii) saturation, or the so-called soft clipping (change of the curvature of the peaks of the signal), which introduces both odd and even harmonics. These effects stem from the linear and nonlinear parts of the mooring load, respectively. Similar phenomena are commonly recognised in the nonlinear optical/audio signal processing engineering fields. In the high-frequency limit, the Expected Value of both ICR coordinates approaches zero. In the low-frequency limit, $E(x_{ICR})$ tends toward negative infinity, and $E(z_{ICR})$ tends toward positive infinity, corresponding to pure translation.

Finally, the ICR excited by irregular waves is sensitive to peak period (frequency) with a trend opposite to that observed for the regular waves. At high frequencies, the ICR in irregular waves aligns with that of regular waves. In an irregular sea state, statistically significant sensitivity of ICR to wave amplitude was not observed due to the contributions from multiple component waves of different frequencies and the relatively lower ("averaged-out") influence of the nonlinear effects.

5. Future work

The work presented in this paper will be continued by investigating the impact of the steady and turbulent wind, to have a better understanding of the rotational behaviour in a real environment. Also, the practical (design and operation/control) implications of the presented findings will be explored further, in particular looking at the impact of the fairlead position on the ICR and the opportunities for a better mooring design. An experimental study should be performed to refine and validate the results.

CRediT authorship contribution statement

Katarzyna Patryniak: Conceptualization, Investigation, Writing – original draft. **Maurizio Collu:** Conceptualization, Writing – review & editing, Supervision. **Andrea Coraddu:** Conceptualization, Writing – review & editing, Supervision.

Declaration of competing interest

The authors declare that they have no known competing financial interests or personal relationships that could have appeared to influence the work reported in this paper.

Appendix A

Figs. 15 and 16 present the time histories of x_{ICR} and z_{ICR} for two wave periods (10 s and 125 s), and for four wave heights (2 m, 4 m, 4 m). Significant differences in the sensitivity of the ICR to the wave height is seen between the two periods' cases. The vast discrepancies at low-frequency (right) are not seen in the ICR history in the high-frequency case (left).

Appendix B

Fig. 17 compares pitch motion time history in a 2 DOF coupled motion (surge and pitch) against a 1 DOF (pitch only) uncoupled motion. Without the coupling, the pitch motion is not distorted and follows a sinusoidal pattern.
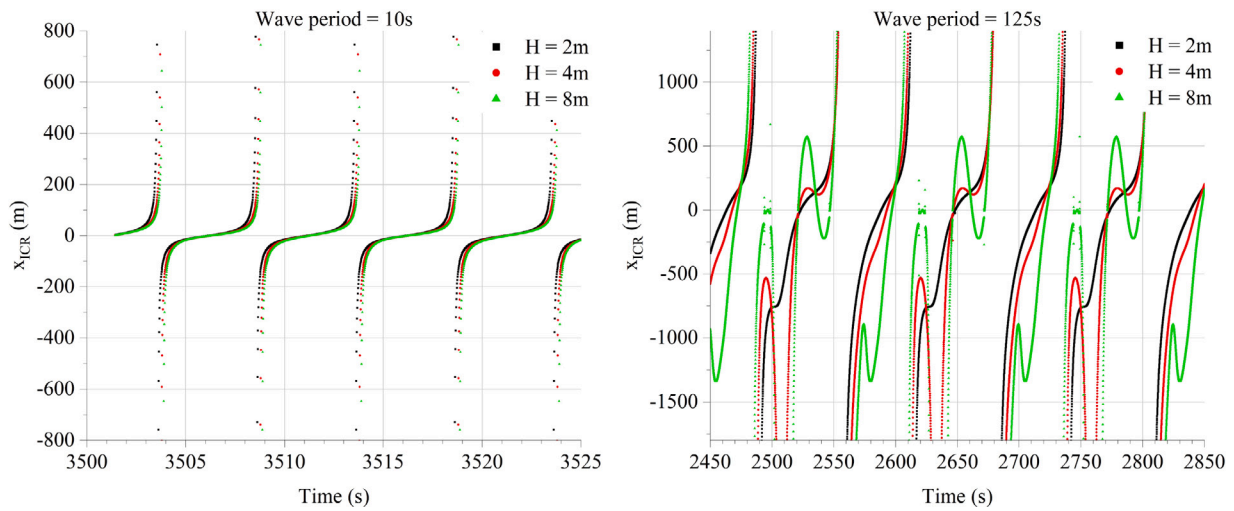
Fig. 15. x-coordinate of ICR as excited by high-frequency (left) and low-frequency (right) waves of three different heights.
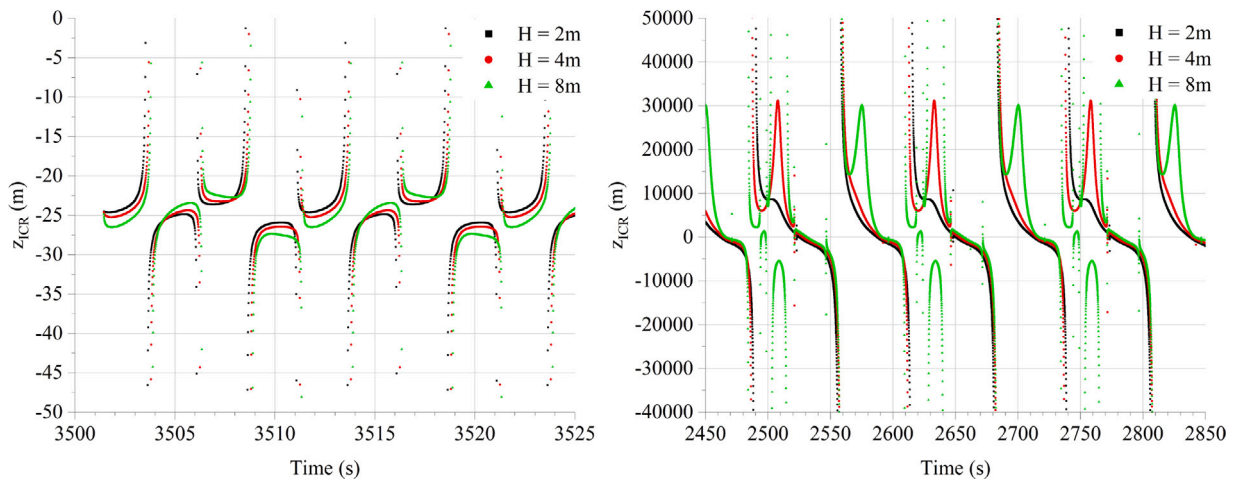

Fig. 16. z-coordinate of ICR as excited by high-frequency (left) and low-frequency (right) waves of three different heights.
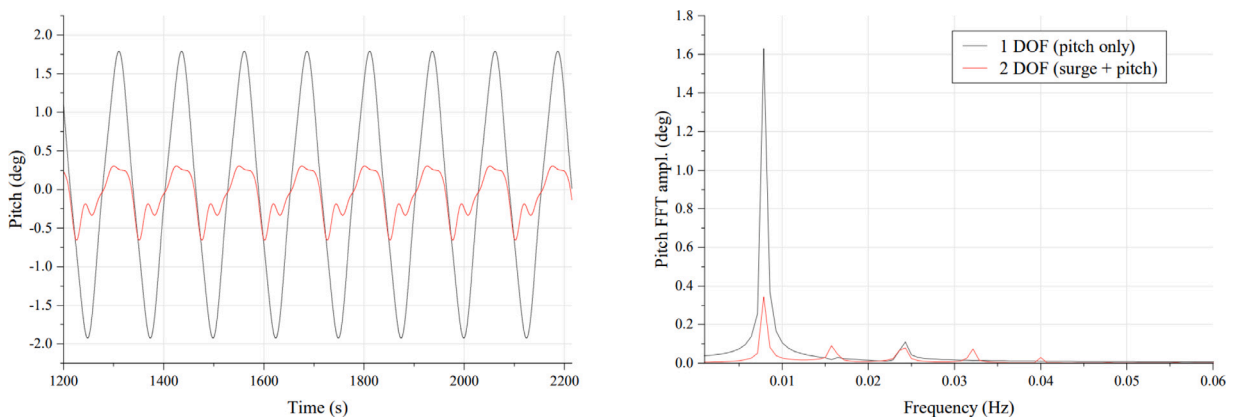

Fig. 17. A comparison of pitch motion time history and FFT amplitudes in a 2 DOF coupled motion against a 1 DOF uncoupled motion.

References

[1] IRENA, Global energy transformation: A roadmap to 2050 (2019 edition), 2019.

[2] GWEC, Global Wind Report 2022, 2022.

[3] A. Myhr, C. Bjerkseter, A. Ågotnes, T.A. Nygaard, Levelised cost of energy for offshore floating wind turbines in a lifecycle perspective, Renew. Energy 66 (2014).

[4] W. Shi, L. Zhang, M. Karimirad, C. Michailides, Z. Jiang, X. Li, Combined effects of aerodynamic and second-order hydrodynamic loads for floating wind turbines at different water depths, Appl. Ocean Res. 130 (2023).

[5] L. Wang, A. Robertson, J. Jonkman, Y.-H. Yu, OC6 phase I: Improvements to the OpenFAST predictions of nonlinear, low-frequency responses of a floating offshore wind turbine platform, Renew. Energy 187 (2022) 282–301.

[6] R. Bergua, A. Robertson, J. Jonkman, E. Branlard, A. Fontanella, M. Belloli, P. Schito, A. Zasso, G. Persico, A. Sanvito, E. Amet, C. Brun, G. Campaña-Alonso, R.

Martín-San-Román, R. Cai, J. Cai, Q. Qian, W. Maoshi, A. Beardsell, G. Pirrung, N. Ramos-García, W. Shi, J. Fu, R. Corniglion, A. Lovera, J. Galván, T.A. Nygaard, C.R. dos Santos, P. Gilbert, P.-A. Joulin, F. Blondel, E. Frickel, P. Chen, Z. Hu, R. Boisard, K. Yilmazlar, A. Croce, V. Harnois, L. Zhang, Y. Li, A. Aristondo, I. Mendikoa Alonso, S. Mancini, K. Boorsma, F. Savenije, D. Marten, R. Soto-Valle, C. Schulz, S. Netzband, A. Bianchini, F. Papi, S. Cioni, P. Trubat, D. Alarcon, C. Molins, M. Cormier, K. Brüker, T. Lutz, Q. Xiao, Z. Deng, F. Haudin, A. Goveas, OC6 project phase III: Validation of the aerodynamic loading on a wind turbine rotor undergoing large motion caused by a floating support structure, Wind Energy Sci. Discuss. 2022 (2022).

[7] B. Wen, Z. Li, Z. Jiang, X. Tian, X. Dong, Z. Peng, Floating wind turbine power performance incorporating equivalent turbulence intensity induced by floater oscillations, Wind Energy 25 (2) (2022) 260–280.

[8] G. Chen, X.-F. Liang, X.-B. Li, Modelling of wake dynamics and instabilities of a floating horizontal-axis wind turbine under surge motion, Energy 239 (2022).

[9] W. Liu, W. Luo, M. Yang, X. Tianyu, Y. Huang, S. Wang, J. Leng, Y. Li, Development of a fully coupled numerical hydroelasto-plastic approach for offshore structure, Ocean Eng. 258 (2022).

[10] V. Leroy, S. Delacroix, A. Merrien, E. Bachynski-Polić, J.-C. Gilloteaux, Experimental investigation of the hydro-elastic response of a spar-type floating offshore wind turbine, Ocean Eng. 255 (2022).

[11] M. Verma, M.K. Nartu, A. Subbulakshmi, Optimal TMD design for floating offshore wind turbines considering model uncertainties and physical constraints, Ocean Eng. 243 (2022).

[12] D. Zalkind, N.J. Abbas, J. Jasa, A. Wright, P. Fleming, Floating wind turbine control optimization, J. Phys. Conf. Ser. 2265 (4) (2022).

[13] L. Meriam, G. Kraige, Engineering Mechanics, Volume 2, Dynamics, seventh ed., John Wiley & Sons, Inc., 1993.

[14] A.C. Fernandes, P. Asgari, A.R. Soares, Asymmetric roll center of symmetric body in beam waves, Ocean Eng. 112 (2016) 66–75.

[15] P. Esperança, J. Sales, S. Liapis, J.P. Matsuura, W. Schott, An experimental investigation of roll motions of an FPSO, in: Proceedings of the International Conference on Offshore Mechanics and Arctic Engineering - OMAE, Vol. 1, 2008.

[16] R. Standing, Prediction of viscous roll damping and response of transportation barges in waves, in: International Ocean and Polar Engineering Conference, 1991.

[17] W.P. Stewart, W.A. Ewers, Wave induced motions of marine deck cargo barges, in: Second International Conference on Behaviour of Off-Shore Structures, BOSS'79, Imperial College, London, 1979.

[18] H.A. Haslum, O.M. Faltinsen, Simplified methods applied to nonlinear motion of spar platforms (A thesis submitted in partial fulfilment of the requirements for the degree of Doktor Ingenipr. Trondheim, 2000).

[19] F. Souza, R. Anderson, A. Oliveira, A. Fernandes, Influência do Centro de Rotação através de Ensaios de Decaimento no Movimento de Balanço Transversal de Cascos Típicos de FPSO (in Portuguese), XXIV Congresso Nacional de Transportes Marítimos e Construção Naval e Offsh.

[20] D. Costa, A.C. Fernandes, J.S. Sales Junior, P. Asgari, Instantaneous center of rotation in pitch response of a FPSO submitted to head waves, in: International Conference on Offshore Mechanics and Arctic Engineering, Volume 7A: Ocean Engineering, 2018.

[21] D. Costa, A.C. Fernandes, J.S. Sales Junior, Further study on the instantaneous rotation center in pitch and its distribution in space for a moored vessel submitted to head regular waves, Ocean Eng. 218 (2020).

[22] D. Costa, J.S. Sales Junior, A.C. Fernandes, Instantaneous center of rotation of a vessel submitted to oblique waves, in: International Conference on Offshore Mechanics and Arctic Engineering, Volume 6B: Ocean Engineering, 2020.

[23] A. Couto, P. Justino, T. Simões, A. Estanqueiro, Impact of the wave/wind induced oscillations on the power performance of the WindFloat wind turbine, J. Phys. Conf. Ser. 2362 (2022).

[24] B. Wen, Z.-W. Li, Z. Jiang, X. Tian, X.-J. Dong, Z. Peng, Floating wind turbine power performance incorporating equivalent turbulence intensity induced by floater oscillations, Wind Energy 25 (2022).

[25] L. Souza Pinheiro Da Silva, M. de Oliveira, B. Cazzolato, N. Sergiienko, G. do Amaral, B. Ding, Statistical linearisation of a nonlinear floating offshore wind turbine under random waves and winds, Ocean Eng. 261 (2022).

[26] T. Tran, D. Kim, J. Song, Computational fluid dynamic analysis of a floating offshore wind turbine experiencing platform pitching motion, Energies 7 (2014) 5011–5026.

[27] Y. Liu, Q. Xiao, A. Incecik, C. Peyrard, D. Wan, Establishing a fully coupled CFD analysis tool for floating offshore wind turbines, Renew. Energy 112 (2017) 280–301.

[28] F. Kelberlau, Free decay testing of a semisubmersible offshore floating platform for wind turbines in model scale (Master's thesis).

[29] L. Eliassen, Aerodynamic loads on a wind turbine rotor in axial motion, https://core.ac.uk/display/30846862?source=4.

[30] M. Kaptan, B. Skaare, Z. Jiang, M.C. Ong, Analysis of spar and semi-submersible floating wind concepts with respect to human exposure to motion during maintenance operations, Mar. Struct. 83 (2022).

[31] K. Stewart, Expected value. Encyclopedia britannica, 2022, https://www.britannica.com/topic/expected-value, (Accessed 24 October 2022).

[32] OpenFAST v2.6, 2021, URL https://github.com/openfast/openfast/, (Accessed: May 4, 2023).

[33] C.H. Lee, J.N. Newman, WAMIT user manual, versions 6.4, Tech. rep., Massachusetts Institute of Technology, 2006, URL https://wamit.com/.

[34] M.D. Masciola, MAP++ mooring analysis program, 2022, https://www.nrel.gov/wind/nwtc/map-plus-plus.html, (Accessed 13/12/2022).

[35] M. Masciola, J. Jonkman, A. Robertson, Implementation of a multisegmented, quasi-static cable model, in: International Ocean and Polar Engineering Conference, 2013.

[36] A. Fernandes, P. Asgari, S. Seddigh, Roll center of a FPSO in regular beam seas for all frequencies, 2015.

[37] J.N. Newman, Marine Hydrodynamics, 40th Anniversary Edition, second ed., The MIT Press Cambridge, Massachusetts, London, England, 2018.

[38] O. Faltinsen, Sea Loads on Ships and Offshore Structure, Cambridge University Press, 1993.

[39] E.V. Lewis, Principles of Naval Architecture. Volume III. Motions in Waves and Controllability, second ed., The Society of Naval Architects and Marine Engineers, Jersey City, NJ, 1989.

[40] DNV GL, Recommended practice — DNVGL RP C205. Edition September 2019, amended December 2019.

[41] J. Jonkman, Definition of the floating system for phase IV of OC3, Tech. rep., National Renewable Energy Laboratory (NREL), 2010.

[42] J. Jonkman, S. Butterfield, W. Musial, G. Scott, Definition of a 5-MW reference wind turbine for offshore system development, 2009.

[43] IEC, Technical Specification IEC 61400-3:2009. Wind turbines – Part 3: Design requirements for offshore wind turbines, Tech. rep., International Electrotechnical Commission, 2009, URL https://webstore.iec.ch/publication/7037.

[44] E.C. Tupper, Introduction to Naval Architecture, fourth ed., Elsevier, 2004.

[45] E.V. Lewis, Principles of Naval Architecture, 2nd revision, Society of Naval Architects and Marine Engineers, Jersey City, N.J., 1988.

[46] D.T. Brown, Chapter 8 - mooring systems, in: S.K. Chakrabarti (Ed.), Handbook of Offshore Engineering, Elsevier, London, 2005, pp. 663–708.

[47] C.E.S. Souza, E.E. Bachynski, Changes in surge and pitch decay periods of floating wind turbines for varying wind speed, Ocean Eng. 180 (2019) 223–237.

[48] G. do Amaral, P. Mello, L. Souza do Carmo, I. Alberto, E. Malta, A. Simos, G. Franzini, H. Suzuki, R. Gonçalves, Seakeeping tests of a FOWT in wind and waves: An analysis of dynamic coupling effects and their impact on the predictions of pitch motion response seakeeping tests of a FOWT in wind and waves: An analysis of dynamic coupling effects and their impact on the predictions of pitch motion, J. Mar. Sci. Eng. 9 (2021).

[49] L.E. Borgman, The spectral density for ocean wave forces, 1967.

[50] A.N. Robertson, S. Gueydon, E. Bachynski, L. Wang, J. Jonkman, D. Alarcón, E. Amet, A. Beardsell, P. Bonnet, B. Boudet, C. Brun, Z. Chen, M. Féron, D. Forbush, C. Galinos, J. Galvan, P. Gilbert, J. Gómez, V. Harnois, F. Haudin, Z. Hu, J.L. Dreff, M. Leimeister, F. Lemmer, H. Li, G. Mckinnon, I. Mendikoa, A. Moghtadaei, S. Netzband, S. Oh, A. Pegalajar-Jurado, M.Q. Nguyen, K. Ruehl, P. Schünemann, W. Shi, H. Shin, Y. Si, F. Surmont, P. Trubat, J. Qwist, S. Wohlfahrt-Laymann, OC6 Phase I: Investigating the underprediction of low-frequency hydrodynamic loads and responses of a floating wind turbine, J. Phys. Conf. Ser. 1618 (3) (2020).

[51] A. Srinivas, B. Robertson, J.B. Gadasi, B.G. Simpson, P. Lomónaco, J.M.B. Ilzarbe, Impact of limited degree of freedom drag coefficients on a floating offshore wind turbine simulation, J. Mar. Sci. Eng. 11 (2023).

[52] A. Alping, G. Jacobsen, Effects of Clipping and Limiting on the Performance of Optical Fiber Communication Systems, Vol. 32, 2014, pp. 2307–2316.

[53] U. Zölzer, AD/DA Conversion, John Wiley & Sons, Ltd, 2011, pp. 63–96.